Engineering Geology 260 (2019) 105218

Contents lists available at ScienceDirect

Engineering Geology

journal homepage: www.elsevier.com/locate/enggeo

Earth pressure profiles in unsaturated soils under transient flow

Shahriar Shahrokhabadi[a,b], Farshid Vahedifard[a,*], Ehsan Ghazanfari[c], Maziar Foroutan[c]

[a] Dept. of Civil and Environmental Engineering, Mississippi State Univ., Mississippi State, MS 39762, USA
[b] Intertek-PSI, 2930 Eskridge Rd., Fairfax, VA 22031, USA
[c] Dept. of Civil and Environmental Engineering, Univ. of Vermont, Burlington, VT 05405, USA

ARTICLE INFO

Keywords:
Unsaturated soil
Effective stress
Active earth pressure
Passive earth pressure
At-rest earth pressure
Transient flow

ABSTRACT

Assessing the effect of heavy precipitations on earthen structures warrants studying earth pressure profiles in unsaturated soils under transient flow. This paper presents an analytical framework to determine the changes in at-rest, active, and passive earth pressures of unsaturated soils due to transient infiltration. A closed-from solution for one-dimensional transient unsaturated flow is incorporated into a suction stress-based representation of effective stress to obtain the tempo-spatial changes in matric suction, suction stress, and effective stress. The profiles are used to extend Hooke's law and Rankine's earth pressure theory, leading to the determination of unsaturated at-rest, active, and passive earth pressures at different depths and times. The analytical framework is used in a set of parametric study for three hypothetical soils of clay, silt, and fine sand. The results reveal the nonlinear characteristics of earth pressure profiles during transient infiltration for all three soils, whereas a linear trend is generally seen under steady-state flow conditions. Further, the depth of tension crack under transient flow is different than the one resulted from steady-state analysis. A transition from tension to compression stress is seen near the soil surface. This observation can be particularly important for fine-grained soils, implying that the depth of tension zone is affected by suction stress changes. Findings of this study can contribute toward a better understanding of service state behavior and forensic studies of earthen structures under heavy precipitations.

1. Introduction

Heavy precipitations threaten the integrity of natural and man-made slopes, embankments, and earthen structures. Rainfall-triggered landslides in natural slopes annually cause multi-billion dollars of damage and several dozens of deaths in the United Sates and other regions of the world (e.g., Larsen, 2008; Sorbino and Nicotera, 2013; Petley, 2012; Bordoni et al., 2015; Ering and Babu, 2016; Gariano and Guzzetti, 2016; Tang et al., 2018). Several failures of slopes and earthen structures occurred when the soil was subjected to varying degrees of saturation (e.g., Rahardjo et al., 2012; Godt et al., 2009; Rahimi et al., 2010; Kim and Borden, 2013; Yoo and Jung, 2006; Godt et al., 2012; Leshchinsky et al., 2015; Oh and Lu, 2015; Pham et al., 2018; Yang et al., 2018). This observation demonstrates the need for assessing the time-dependent response of slopes and earthen structures under variably saturated flow conditions. This aspect is equally critical for different related fields including engineering geology, geotechnical engineering and civil engineering. The need is more pronounced considering that historical observations (e.g., USGCRP (U.S. Global Change Research Program), 2009; IPCC, 2013) show a notable increase in intensity and frequency of heavy precipitations, partly attributed to anthropogenic climate change. Adapting infrastructure to climate change requires quantitative assessments of the impacts of new patterns of extreme precipitations on the performance of slopes and earthen structures (e.g., NRC, 2013; Vardon, 2015; CACC (Committee on Adaptation to a Changing Climate), 2015; Jasim et al., 2017; Robinson et al., 2017; CACC (Committee on Adaptation to a Changing Climate), 2018; Vahedifard et al., 2017a, 2018; Ragno et al., 2018).

Design and analysis of earth retaining structures are primarily performed using earth pressure theories (e.g., Rankine, Coulomb). Design guidelines for earth retaining structures (e.g., Federal Highway Administration (FHWA), 2009; AASHTO, 2014) are developed based on classic soil mechanics, where the soil is treated as either dry or fully saturated. Previous studies have demonstrated that negative pore-water pressure, or matric suction, can notably contribute, in some cases significantly, to shear strength leading to a reduction in the lateral thrust of the backfill (e.g., Vahedifard et al., 2015, 2016). However, current design guidelines commonly ignore the contribution of matric suction

* Corresponding author.
E-mail addresses: s.shahrokhabadi@Intertek.com (S. Shahrokhabadi), farshid@cee.msstate.edu (F. Vahedifard), Ehsan.Ghazanfari@uvm.edu (E. Ghazanfari), Maziar.Foroutan@uvm.edu (M. Foroutan).

https://doi.org/10.1016/j.enggeo.2019.105218
Received 10 January 2019; Received in revised form 27 June 2019; Accepted 3 July 2019
Available online 05 July 2019

in the design of earth retaining structures. Neglecting the matric suction role in design is a legitimate and safe practice, considering the uncertainties associated with variation of matric suction during the life span of the structure (e.g., Leshchinsky and Tatsuoka, 2013; Vahedifard et al., 2014). At the same time, understanding the true service state behavior of earth retaining structures warrants considering unsaturated soil mechanics in the analysis of these structures. This can lead to more realistic assessments of the earthen structures response under the field conditions, particularly when subjected to extreme loadings (e.g., heavy precipitations). In such cases, matric suction and, subsequently, shear strength in the unsaturated zone are affected by the intensity and duration of precipitation (e.g., Robinson et al., 2017; Lu and Godt, 2013). This time-dependent variation of matric suction and shear strength can increase the lateral earth pressure, adversely affecting the integrity of structures (Chen, 1988; Nelson and Miller, 1992; Blake et al., 2003; Vahedifard et al., 2017b; Yang et al., 2018).

Several numerical, analytical, and experimental studies have been performed to investigate the effect of matric suction on earth pressures under at-rest, active, and passive modes (e.g., Zhang et al., 2009; Yelti, 2011; Oh et al., 2013; Li et al., 2014; Vo and Russell, 2014; Monoroy et al., 2015; Vo et al., 2016; Sahoo and Ganesh, 2017; Li and Yang, 2018). For modeling purposes, hydro-mechanical numerical simulations (e.g., using finite element, or finite difference method) are needed to properly capture tempo-spatial distribution of earth pressures under variably saturated transient flow conditions (e.g., Vahedifard et al., 2017b; Zhang et al., 2016; Yang et al., 2018). As a less complex yet reliable alternative, analytical methods can provide an accurate and practical measure to determine lateral pressures of unsaturated soils. Several attempts have been made to extend classic earth pressure theories (e.g., Rankine, Coulomb, Hooke's law) to unsaturated soils by employing either Bishop (1959)'s effective stress expression (e.g., Lu and Likos, 2004; Zhang et al., 2010) or Fredlund and Morgenstern (1977)'s independent stress state variables approach (e.g., Fredlund and Rahardjo, 1993; Zhang et al., 2010; Liang et al., 2012). Few studies (e.g., Lu and Likos, 2004; Vahedifard et al., 2015; Li and Yang, 2018) accounted for flux boundary characteristics in the solution by incorporating an analytical solution describing one-dimensional unsaturated flow into their earth pressure formulation. However, all these studies only consider steady-state unsaturated flow, suitable for assigning earth pressures under long term loading conditions.

This paper presents an analytical framework to capture the variation of active, at-rest, and passive earth pressures of unsaturated soils due to transient infiltration. A closed-from solution for one-dimensional transient unsaturated flow, proposed by Srivastava and Yeh (1991), is incorporated into a suction stress-based representation of effective stress (Lu and Likos, 2006; Lu et al., 2010) to obtain matric suction, suction stress, and shear strength. Exponential functional forms are used to represent the Soil Water Retention Curve (SWRC) and Hydraulic Conductivity Function (HCF) in the formulations. The resulting profiles are used to extend Hooke's law and Rankine's earth pressure theory, leading to the determination of transient at-rest, active, and passive earth pressure profiles for unsaturated soils. The proposed analytical framework is used in a set of parametric study for three hypothetical soils of clay, silt, and fine sand. To the best of the authors' knowledge, this work is the first attempt to develop an analytical solution for unsaturated earth pressure profiles under transient flow. The proposed framework provides a useful and robust tool for assessing the effect of transient infiltration on the service state behavior and forensic studies of unsaturated earth retaining structures.

2. Effective stress in unsaturated soils

We use the suction stress-based representation of effective stress outlined by Lu and Likos (2004, 2006) in this study. Building upon Bishop (1959)'s effective stress expression, the effective stress for both saturated and unsaturated soils can be defined as (Lu and Likos, 2004, 2006):

$$\sigma' = (\sigma - u_a) - \sigma^s \tag{1}$$

where σ and σ' are the total and effective stress, respectively, σ^s represents the suction stress, and u_a represents the pore-air pressure, which is assumed to be equal to the atmospheric pressure and set to zero in this study ($u_a = 0$). Lu et al. (2010) defined σ^s for both saturated and unsaturated soils as:

$$\sigma^s = -(u_a - u_w) \qquad if\ (u_a - u_w) < 0 \tag{2.a}$$

$$\sigma^s = -S_e(u_a - u_w) \qquad if\ (u_a - u_w) \geq 0 \tag{2.b}$$

$$S_e = \frac{\theta - \theta_r}{\theta_s - \theta_r} \tag{2.c}$$

where u_w is the pore-water pressure, S_e is the effective degree of saturation, θ is the volumetric water content, θ_r is the residual volumetric water content, and θ_s is the saturated volumetric water content. The term $(u_a - u_w)$ represents the matric suction.

3. Analytical solution for transient flow in unsaturated soils

Richards' equation (Richards, 1931) is commonly employed as the governing equation to describe transient fluid flow in unsaturated soils. It is noted that there are other alternative methods in the literature for this purpose. For example, Pudasaini (2016) presented a new sub-diffusion and sub-advection model to describe the fluid flow in porous and debris materials and showed that the model developed therein better describes the fluid flow in porous media than the earlier classic methods. The Pudasaini (2016) model is derived fully mechanically and does not require any fitting parameters, which is the case in classic methods such as those proposed by Dupuit (1863) and Richards (1931).

In this study, we use the closed-from solution proposed by Srivastava and Yeh (1991) for one-dimensional form of Richards' equation to obtain the matric suction at different depths and times. The resulting matric suction profiles are then incorporated into the effective stress formulations outlined in the previous section. It is noted that a similar approach is used by others for stability analysis of unsaturated slopes under transient flow (e.g., Baum et al., 2008; Godt et al., 2012; Lu and Godt, 2013).

The one-dimensional form of Richards' equation can be written as:

$$\frac{\partial \theta}{\partial t} = \frac{\partial}{\partial z}\left[k(h_m)\frac{\partial(h_m - z)}{\partial z}\right] \tag{3}$$

where h_m is the suction head and is equal to $\left(\frac{u_a - u_w}{\gamma_w}\right)$ and z is the vertical coordinate, where the origin is located at the water table depth and the upward direction is considered positive.

Eq. (3) is a highly nonlinear equation, which can be linearized using Gardner, 1958 (1985)'s exponential model for the SWRC and HCF. Gardner's model relies only on one fitting parameter, α, which represents the vertical height of the capillary fringe. Owing to its simple functional form and reasonable accuracy, Gardner's model is widely used in literature, particularly in analytical derivations (e.g., Yeh, 1989; Srivastava and Yeh, 1991; Lu and Likos, 2004; Lu and Godt, 2013). The HCF based on Gardner's model can be written as:

$$k = k_s e^{-\alpha\gamma_w h_m} \tag{4}$$

where k is the hydraulic conductivity and k_s is the saturated hydraulic conductivity. The extension of Gardner's definition for the SWRC establishes a relationship between degree of saturation and matric suction as:

$$S_e = e^{-\alpha\gamma_w h_m} \tag{5}$$

One can linearize Richards' equation by implementing Eq. (4) and Eq. (5) into Eq. (3):

$$\frac{\alpha(\theta_s - \theta_r)}{k_s}\frac{\partial k}{\partial t} = \frac{\partial^2 k}{\partial z} - \alpha\frac{\partial k}{\partial z} \tag{6}$$

It is required to define one initial and two boundary conditions to obtain a particular solution of Eq. (6). In this study, it is assumed the soil layer (domain) is exposed to a constant infiltration rate at the soil surface while zero pore-water pressure (suction) is imposed on the lower boundary. The initial suction head (h_{m0}) is distributed linearly within the domain from H at the soil surface to zero at the lower boundary where H represents the depth of water table from the ground surface (which is equal to the thickness of the domain for the imposed boundary conditions).

We introduce the following dimensionless variables:

$$Z = \alpha z \qquad k^* = \frac{k}{k_s} \qquad L = \alpha H \qquad Q = \frac{q}{k_s} \qquad T = \frac{\alpha k_s t}{\theta_s - \theta_r}$$

where q is the prescribed flux at the soil surface with respect to times >0. Then, Eq. (6) can be rewritten in the following form:

$$\frac{\partial k^*}{\partial T} = \frac{\partial^2 k^*}{\partial Z^2} + \frac{\partial k^*}{\partial Z} \tag{7}$$

Consequently, the initial and boundary conditions are represented as:

$$k^*(Z,0) = e^{-Z} = k_0^*(Z) \tag{8a}$$

$$k^*(0,T) = 1 \tag{8b}$$

$$\left[\frac{\partial k^*}{\partial Z} + k^*\right]_{Z=L} = Q \tag{8c}$$

Applying the Laplace transform to Eq. (7) along with the initial boundary condition (Eq. (8a)), zero pore-water pressure (or suction) at Z = 0 (Eq. (8b)), and the prescribed constant flux infiltration (Eq. (8c)), we obtain:

$$\frac{\partial^2 \overline{k^*}}{\partial Z^2} + \frac{\partial \overline{k^*}}{\partial Z} - S\overline{k^*} + k_0^* = 0 \tag{9}$$

where is the transformation of k^* and the corresponding boundary conditions are presented as:

$$\overline{k^*}(0) = \frac{1}{S} \tag{10a}$$

$$\left[\frac{\partial \overline{k^*}}{\partial Z} + \overline{k^*}\right]_{Z=L} = \frac{Q}{S} \tag{10b}$$

There is a specific solution $\left(\frac{k_0^*(Z)}{S}\right)$ for the reformed governing equation (Eq. (9)). Given the prescribed the boundary conditions (Eq. (10a) and Eq. (10b)), Srivastava and Yeh (1991) proposed a general solution for Eq. (9) as:

$$\overline{k^*} = \frac{k_0^*(Z)}{S} + Qe^{\frac{L-Z}{2}}F(S) \tag{11a}$$

$$F(S) = \frac{\sinh\left[Z\left(S+\frac{1}{4}\right)^{\frac{1}{2}}\right]}{S\left\{\frac{1}{2}\sinh\left[L\left(S+\frac{1}{4}\right)^{\frac{1}{2}}\right] + \left(S+\frac{1}{4}\right)^{\frac{1}{2}}\cosh\left[L\left(S+\frac{1}{4}\right)^{\frac{1}{2}}\right]\right\}} \tag{11b}$$

The inversion of $F(S)$ is obtained by using the residue theorem (Özışık, 1980) as the sum of residues of $e^{ST}F(S)$ at the poles of $F(S)$. The poles can be obtained by setting $\left(S+\frac{1}{4}\right)^{\frac{1}{2}}$ as a complex number. It is noted that all the poles are imaginary values of $\left(S+\frac{1}{4}\right)^{\frac{1}{2}}$, which are obtained as the positive roots of the pseudoperiodic characteristic equation:

$$\tan(\lambda_n L) + 2\lambda_n = 0 \tag{12}$$

where λ_n is the n^{th} root of Eq. (12). Srivastava and Yeh (1991) defined the dimensionless hydraulic conductivity as:

$$k^* = Q - (Q-1)e^{-Z} - 4Qe^{\frac{(L-Z)}{2}}e^{\frac{-T}{4}}\sum_{n=1}^{\infty}\frac{\sin(\lambda_n Z)\sin(\lambda_n L)e^{-\lambda_n^2 T}}{1+\frac{L}{2}+2\lambda_n^2 L} \tag{13}$$

where L is the dimensionless depth of the water table below the ground surface. Determining $k^*$is a key step toward finding suction head within the problem domain. Using k^* calculated from Eq. (13) along with Gardner's HCF (Eq. (4)), one can determine h_m via:

$$h_m = \frac{-ln(k^*)}{\alpha\gamma_w} \tag{14}$$

Determining $h_m(z,t)$ enables one to calculate matric suction and suction stress as a function of depth and time (i.e., $\sigma^s(t,z)$).

4. Extended earth pressures under transient flow in unsaturated soils

In this section, the formulations for transient matric suction, suction stress, and effective stress presented in the previous sections are incorporated into Hooke's law and Rankine's earth pressure theory to determine at-rest, active, and passive earth pressures under the transient unsaturated flow condition.

4.1. At-rest earth pressure

Hooke's law is a linear stress-strain constitutive equation, which is commonly used to establish a relationship between vertical and horizontal stress components. Fig. 1 depicts a schematic distribution of vertical and horizontal stress components in an unsaturated soil layer. Hooke's law can be extended to unsaturated soils by incorporating the suction stress-based effective stress representation as follows (Lu and Likos, 2004):

$$\varepsilon_x = \frac{\sigma_x - u_a}{E} - \frac{\mu}{E}(\sigma_y + \sigma_z - 2u_a) - \frac{1-2\mu}{E}\sigma^s \tag{15.a}$$

$$\varepsilon_y = \frac{\sigma_y - u_a}{E} - \frac{\mu}{E}(\sigma_x + \sigma_z - 2u_a) - \frac{1-2\mu}{E}\sigma^s \tag{15.b}$$

$$\varepsilon_z = \frac{\sigma_z - u_a}{E} - \frac{\mu}{E}(\sigma_x + \sigma_y - 2u_a) - \frac{1-2\mu}{E}\sigma^s \tag{15.c}$$

where ε_x, ε_y and ε_z are elastic strains in the x, y, and z directions, respectively; σ_x, σ_y and σ_z are elastic total stresses in the horizontal and vertical directions, respectively; and E and μ represent Young's modulus and Poisson's ratio, respectively. For a homogenous unsaturated layer in a half-space domain, it is reasonable to consider the following simplifying assumptions (Lu and Likos, 2004):

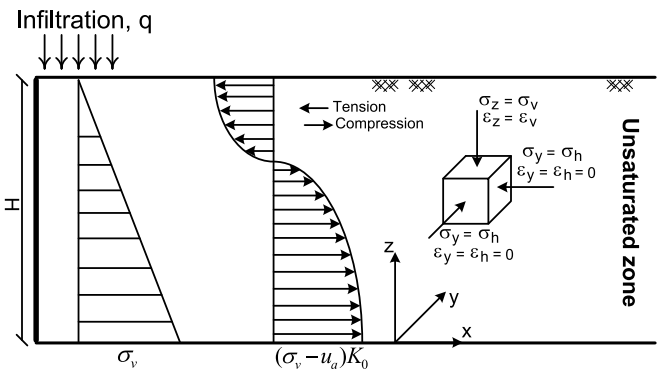

Fig. 1. Vertical and horizontal stresses in half-space unsaturated soil for at-rest condition.

1. The horizontal stresses are equal ($\sigma_x = \sigma_y = \sigma_h$).
2. The horizontal strains are negligible ($\varepsilon_x = \varepsilon_y = \varepsilon_h = 0$).

Imposing the first assumption reduces Eq. (15) to:

$$\varepsilon_v = \frac{\sigma_v - u_a}{E} - \frac{2\mu}{E}(\sigma_h - u_a) - \frac{1-2\mu}{E}\sigma^s \tag{16.a}$$

$$\varepsilon_h = \frac{\sigma_h - u_a}{E} - \frac{\mu}{E}(\sigma_v + \sigma_h - 2u_a) - \frac{1-2\mu}{E}\sigma^s \tag{16.b}$$

Using the second assumption further simplifies Eq. (16) to:

$$\sigma_h - u_a = \frac{\mu}{1-\mu}(\sigma_v - u_a) + \frac{1-2\mu}{1-\mu}\sigma^s \tag{17}$$

Subsequently, by rearranging Eq. (17), the coefficient of at-rest earth pressure for unsaturated soils (K_{0u}) is presented as (Lu and Likos, 2004):

$$K_{0u} = \frac{\sigma_h - u_a}{\sigma_v - u_a} = \frac{\mu}{1-\mu} + \frac{1-2\mu}{1-\mu}\frac{\sigma^s}{(\sigma_v - u_a)} \tag{18}$$

The above equation can be used along with the transient matric suction and suction stress equations presented in the previous sections to determine the coefficient of at-rest earth pressure and earth pressure profile versus the depth at any time.

4.2. Active earth pressure

Rankine's state of failure in the active mode implies that the failure is induced by the soil weight rather than external loads. Rankine's earth pressure theory employs several simplifying assumptions to express the failure in the limit equilibrium analysis. For instance, a frictionless boundary is assumed, which allows the lateral movement of a soil mass and reduces the horizontal stress. Further, this assumption enables one to consider the major and minor principal stresses acting along the vertical and horizontal directions, respectively. Subsequently, implementation of the Mohr-Coulomb failure criterion in the active mode allows defining the stress state at failure as (Lu and Likos, 2004):

$$\sigma_h' = \sigma_v' K_a - 2c'\sqrt{K_a} \tag{19}$$

where σ_h' represents the horizontal effective stress, σ_v' represents the vertical effective stress, c' is the soil's effective cohesion, and K_a is the coefficient of Rankine's active earth pressure, which is defined as:

$$K_a = tan^2\left(\frac{\pi}{4} - \frac{\phi'}{2}\right) \tag{20}$$

For unsaturated soils, one can extend Rankine's active earth pressure by incorporating Eq. (1) into Eq. (19) as follows:

$$(\sigma_h - u_a) = (\sigma_v - u_a)K_a - 2c'\sqrt{K_a} - (K_a - 1)\sigma^s \tag{21}$$

In the above equation, the first two terms in the right-hand side are identical to those in Rankine's classic earth pressure theory, but the third term extends Rankine's theory to unsaturated soils by accounting for the contribution of suction stress (Lu and Likos, 2004). In a homogenous soil, the first term contributes to compressive earth pressure in the backfill or adjacent retaining structures, while the second (contribution of c') and third (contribution of σ^s) terms contribute to tensile stresses due to nature of suction stress. Fig. 2 shows the contribution of each component to the active lateral earth pressure.

In the absence of surcharge, the contribution of soil weight in lateral earth pressure increases linearly with depth. The second term in Eq. (21), which represents the contribution of mobilized cohesion at the failure state, is a constant value along the depth. However, the third component nonlinearly changes with depth and time. Using Eq. (21), the coefficient of active earth pressure for unsaturated soil K_{au} can be defined as (Lu and Likos, 2004):

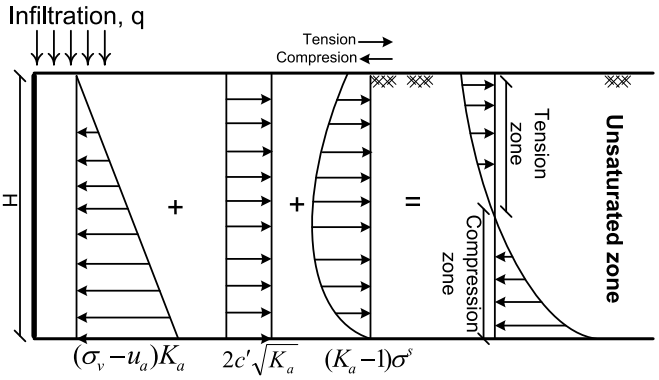

Fig. 2. Contributing components to active earth pressure versus depth due to overburden stress, mobilized cohesion, and suction stress under unsaturated flow.

$$K_{au} = \frac{\sigma_h - u_a}{\sigma_v - u_a} = K_a - \frac{2c'\sqrt{K_a}}{\sigma_v - u_a} - \frac{(K_a - 1)\sigma^s}{\sigma_v - u_a} \tag{22}$$

The role of suction stress component in K_{au} is highlighted when the tension stress appears in the soil body and induces tension cracks. In the tensional cracked zone, the lateral earth pressure is null and the earth pressure profile changes from tension to compression. At this condition, by neglecting u_a, considering K_{au} to be zero at the transition depth, and defining the overburden pressure (σ_v) as γD_t at the depth of tension crack (D_t), one can define:

$$D_t = \frac{2c'}{\gamma\sqrt{K_a}} + \frac{\sigma^s}{\gamma}\left(1 - \frac{1}{K_a}\right) \tag{23}$$

where γ is the soil unit weight. The above equation can be used to estimate the depth of tension zone with suction stress varying with time and depth.

4.3. Passive earth pressure

Passive earth pressure mobilizes in cases such as a soil mass in front of a failing retaining wall or expansive soil mass behind a retaining wall (Lu and Likos, 2004). In the passive earth pressure mode, the horizontal pressure is usually greater than the vertical stress induced by soil weight. Considering the Mohr-Coulomb criterion, the state of failure occurs when the horizontal stress reaches a level that the combination of normal and shear stresses exceeds the failure envelope. The fundamental difference between the passive and active mode of failure lies within the direction of principal stresses. Unlike the active mode, the horizontal effective stress is the maximum principal stress and the vertical stress is the minimum principal stress in the passive mode. The latter characteristics leads to the definition of the passive lateral pressure as:

$$\sigma_h' = \sigma_v' K_p + 2c'\sqrt{K_p} \tag{24}$$

where K_p is the coefficient of Rankine's passive earth pressure defined as:

$$K_p = tan^2\left(\frac{\pi}{4} + \frac{\phi'}{2}\right) \tag{25}$$

For unsaturated soils, Rankine's passive earth pressure can be extended by adding the contribution of suction stress to Eq. (24) as follows:

$$(\sigma_h - u_a) = (\sigma_v - u_a)K_p + 2c'\sqrt{K_p} + (1 - K_p)\sigma^s \tag{26}$$

Subsequently, the extended Rankine's passive earth pressure coefficient for unsaturated soils is derived by dividing the right-hand side of Eq. (26) by the vertical effective stress (Lu and Likos, 2004):

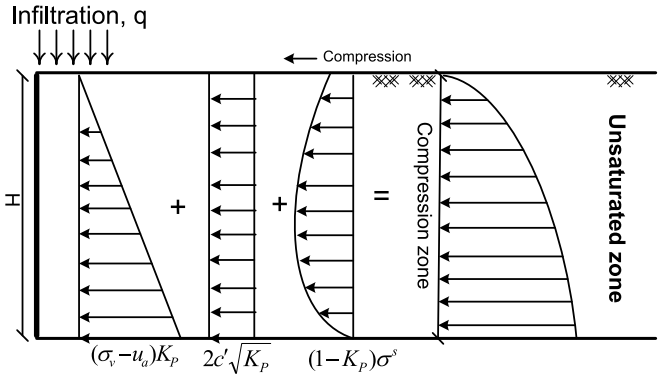

Fig. 3. Contributing components to passive earth pressure versus depth due to overburden stress, mobilized cohesion, and suction stress under unsaturated flow.

$$K_{pu} = \frac{\sigma_h - u_a}{\sigma_v - u_a} = K_p + \frac{2c'\sqrt{K_p}}{\sigma_v - u_a} - \frac{(K_p - 1)\sigma^s}{\sigma_v - u_a} \quad (27)$$

The first two terms in Eq. (27) are the same as those used in Rankine's classic earth pressure theory. The third term, introduced by Lu and Likos (2004), expresses the role of suction stress that can vary nonlinearly with depth and time. In contrast to the active mode, all three terms in the passive mode contribute to compressive earth pressure. Fig. 3 represents a schematic variation of the three components contributing to passive earth pressure with depth. The profiles for the effect of overburden stress, mobilized cohesion, and suction stress versus depth are constant, linear, and nonlinear, respectively. Accounting for the contribution of suction stress leads to a nonlinear profile of passive earth pressure, as well as an overall increase in the magnitude of passive earth pressure.

5. Parametric study

The proposed framework can be employed to assess the effect of various factors on earth pressures of unsaturated soils subjected to the transient flow. In this section we use the formulations in a set of parametric study to determine tempo-spatial distributions of active, at-rest, and passive earth pressures for three hypothetical soils of clay, silt, and fine sand. For each hypothetical soil, the mechanical properties of soil (ϕ', c', unit weight (γ)), are assumed to be constant. Earth pressure profiles are computed for the soils considering two different thicknesses of H = 3 and 6 m. Previous studies (e.g., Lu and Likos, 2004; Vahedifard et al., 2015) have shown a height-dependent behavior for earth pressure profiles in unsaturated soils. These two thicknesses (H = 3 and 6 m) are selected to represent the height range of relatively short to mid-height earthen structures commonly seen in practice. In all cases, the rate of infiltration with respect to the saturated hydraulic conductivity $\left(\frac{q}{k_s}\right)$ is considered to be constant and equal to one. This assumption models the unsaturated layer under a high rate of infiltration, representing extreme precipitations. The initial negative pore-water pressure is assumed to be hydrostatic for all cases, and the pore-air pressure is assumed to be equal to the atmospheric pressure ($u_a = 0$). Table 1 shows the hydrological and mechanical properties of the soils used in the parametric study.

For a given set of input parameters, the following steps are taken to obtain the earth pressure profiles under transient unsaturated flow conditions:

- Employ the closed-from solution for one-dimensional transient unsaturated flow (outlined in Section 3) to obtain the water content and matric suction at each depth and time,
- Use the calculated water content and matric suction to determine the effective degree of saturation (using Eq. (2c)), suction stress (using Eq. (2a) and Eq. (2b)), and effective stress (using Eq. (1)), and
- Use the values determined in the previous step to calculate the transient profiles of at-rest (Eq. (18)), active (Eq. (22)), and passive (Eq. (27)) earth pressures versus depth.

5.1. Clay

Transient flow in clay is a slow process and the pore-water pressure takes a considerably long time to evolve in the soil body. The structure of clay often dominates the corresponding macroscopic strength, deformation, and fluid flow behavior (e.g., Lu and Likos, 2004). The magnitude and behavior of matric suction is a function of the soil properties, degree of saturation, particle size distribution, and air-water interaction (Lu and Likos, 2004).

Using the parameters shown in Table 1, Fig. 4 illustrates the SWRC and HCF of the clay used in the parametric study. Two thicknesses of H = 3 and 6 m for the clay layer subjected to an infiltration rate of $q = 5.0 \times 10^{-8}\ m/s$ are considered. Fig. 5a and b depict the spatial and temporal variation of the normalized negative pore-water pressure (matric suction) and suction stress, respectively. The results are presented from $t = 30$ days until reaching the saturation condition ($u_w = 0$). The results show that the negative pore-water pressure is diminished after 300 and 600 days (not shown) for H = 3 and 6 m, respectively.

Fig. 6a, b, and c show the transient profiles of active, at-rest, and passive earth pressures, respectively, versus depth for the H = 3 m case. Inspection of the transient trends reveals the transition of stress components from tension (negative) to compression (positive) in the active and at-rest modes. The normalized active pressure trend in Fig. 6a shows that approximately 1.8 m of the clay layer experiences tension stress ($\sigma_h < 0$) at $t = 30$ days. At this time, the maximum normalized tension stress is approximately -0.22 near the soil surface. The thickness of the tension zone reduces to about 0.75 m at $t = 300$ days when the soil is fully saturated ($u_w = 0$). The study of active earth pressure at t = 30 and 300 days shows the contribution of suction to tension stress in the soil body, where its influence gradually decreases over time. However, the residual tension stress at t = 300 days and z/H > 0.78 is only induced by the cohesion component, where its normalized magnitude is close to -0.11.

Fig. 6b demonstrates the effect of suction stress on transient at-rest earth pressure analysis. As shown, the thickness of the tension zone is noticeable at t = 30 days, but progressively shrinks to zero near the saturated condition (t = 300 days). While not expected in the classic soil mechanics, Fig. 6b shows the formation of the tension zones, especially in the early stages of infiltration. Fig. 6c represents the role of suction stress in the passive mode, where it shows the suction stress increases the magnitude of passive earth pressure, especially in the

Table 1
Hydrological and mechanical properties of hypothetical soils (data from Lu and Godt, 2013).

Soil	α (1/m)	k_s (m/s)	θ_s	θ_r	c'(kPa)	ϕ'(degrees)	$\gamma\left(\frac{kN}{m^3}\right)$	μ
Clay	0.13	5.0×10^{-8}	0.58	0.05	5	25	18	0.2
Silt	0.5	1.0×10^{-7}	0.45	0.10	1.7	30	20	0.25
Fine sand	0.7	5.0×10^{-6}	0.41	0.05	0.0	35	18	0.25

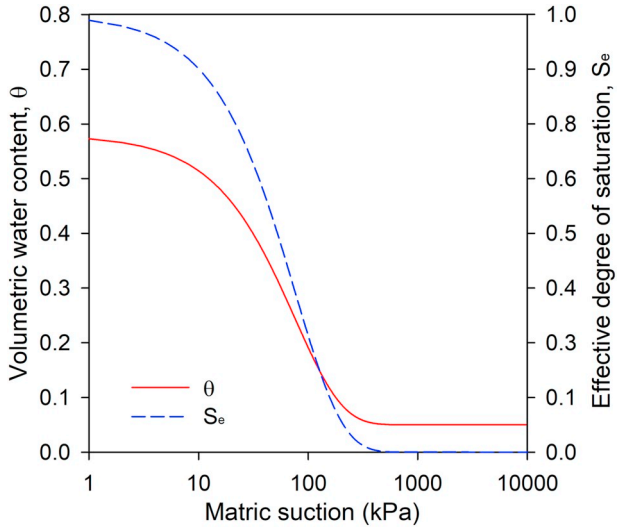

Fig. 4. The SWRC and HCF of clay used in the parametric study.

early stages of infiltration.

Fig. 6d, e, and f represent active, at-rest, and passive earth pressure profiles for clay with H = 6 m. Compared to the results for the H = 3 m case, increasing the thickness of the clay layer to H = 6 m almost doubles the time it takes when the suction is completely diminished. Fig. 6d, e, and f highlight the contribution of suction stress to the formation of a nonlinear shape for the earth pressure profiles. The trends show a nonlinear stress distribution at t = 30 days for all modes (active, at-rest, and passive), which regularly alters to a linear distribution as time marches toward the saturated condition.

5.2. Silt

Similar to clay, the effect of suction stress on transient seepage is critical in silt as the progress of wetting front is a slow process in silt. This example represents the active, at-rest, and passive pressures under transient infiltration for the silt layer with two thicknesses of H = 3 and 6 m. The analysis is performed for a duration of 180 days for H = 3 m and 300 days for H = 6 m at the time intervals of t = 30, 60, 90, 180, and 300 days. Fig. 7 shows the SWRC and HCF used for the silt. The silt layer is exposed to an infiltration rate of $q = 1.0 \times 10^{-7}$ *m/s*.

Fig. 8 represents the results for normalized pore-water pressure (Fig. 8a) as well as the corresponding suction stress (Fig. 8b). The minimum normalized pore-water pressure is about −0.23 and − 0.13 for H = 6 and 3 m at t = 30 days, respectively. The peak values for the normalized pore pressure and suction stress are observed in the middle of the soil layer in a range between z/H = 0.4 to 0.65. Fig. 8b shows a dissimilarity between the normalized suction trend at t = 30 days and the rest of the results for H = 6 m.

In the active earth pressure mode, the likelihood of tension crack formation is high near the soil surface, especially in the absence of surcharge. Therefore, for fine-grained soils it is necessary to consider the effect of cohesion combined with suction stress, which can increase the probability of tension cracks formation within the tension zone. Fig. 9a and d depict the impact of suction stress on the formation of tension zone at the beginning of simulation for H = 3 and 6 m, respectively. The maximum magnitude of normalized active earth pressure in the tension zone is approximately −0.1 and − 0.5 for H = 3 and 6 m, respectively, at t = 30 days. In addition, the tension zone is about 1 and 0.45 m below the surface at t = 30 days. However, the thickness gradually decreases until the soil is fully saturated. Fig. 9b and e suggest a similar trend for at-rest earth pressure profiles. An inspection in the results of the active and at-rest mode shows that the tension zone of the silt is substantially smaller than the tension zone seen in the clay. The evaluation of passive earth pressure profiles (Fig. 9c and f) implies that the trend for passive stress is not time-sensitive, although it slightly decreases with time.

5.3. Fine sand

This section investigates the effect of transient infiltration on the variation of active, at-rest, and passive pressure profiles with time in unsaturated fine sand. Fig. 10 shows the SWRC and HCF used for the fine sand in the parametric study. The fine sand layer with two thicknesses of H = 3 and 6 m is modeled under an infiltration rate of $q = 5.0 \times 10^{-6}$ *m/s*.

Fig. 11 shows the distributions of normalized pore-water pressure (Fig. 11a) and suction stress (Fig. 11b) versus the distance above the water table at different times for the fine sand. Inspection of the results shown in Fig. 11a reveals that the peak pore-water pressure occurs at

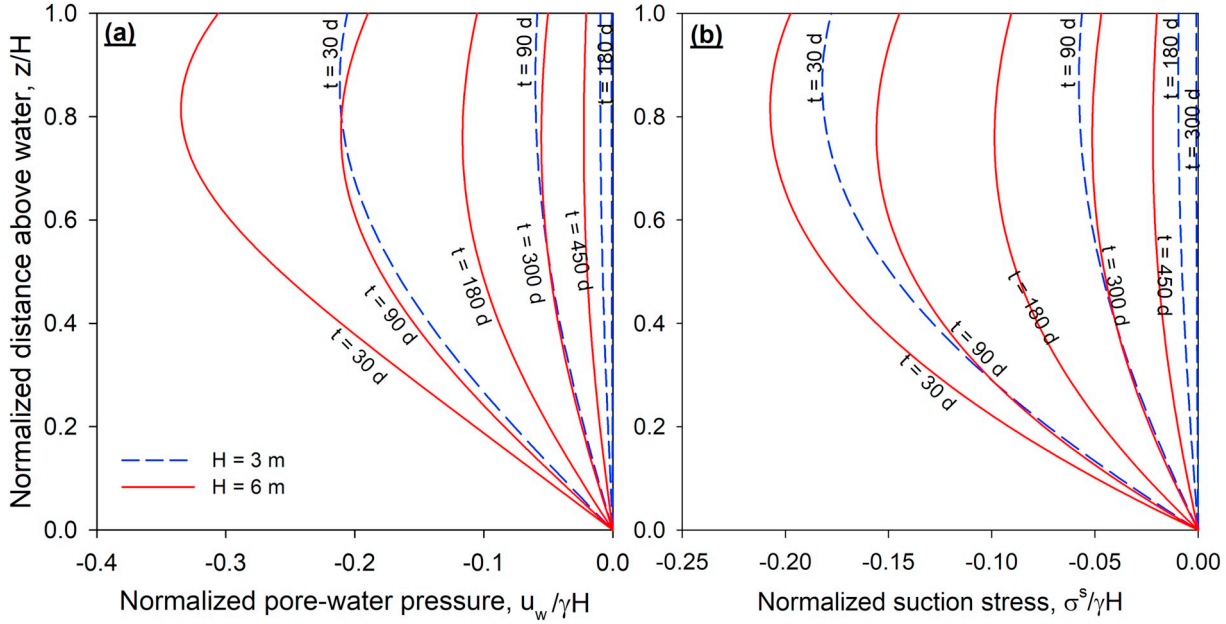

Fig. 5. Transient profiles of normalized distance above the water table in clay versus: (a) normalized pore-water pressure and, (b) normalized suction stress.

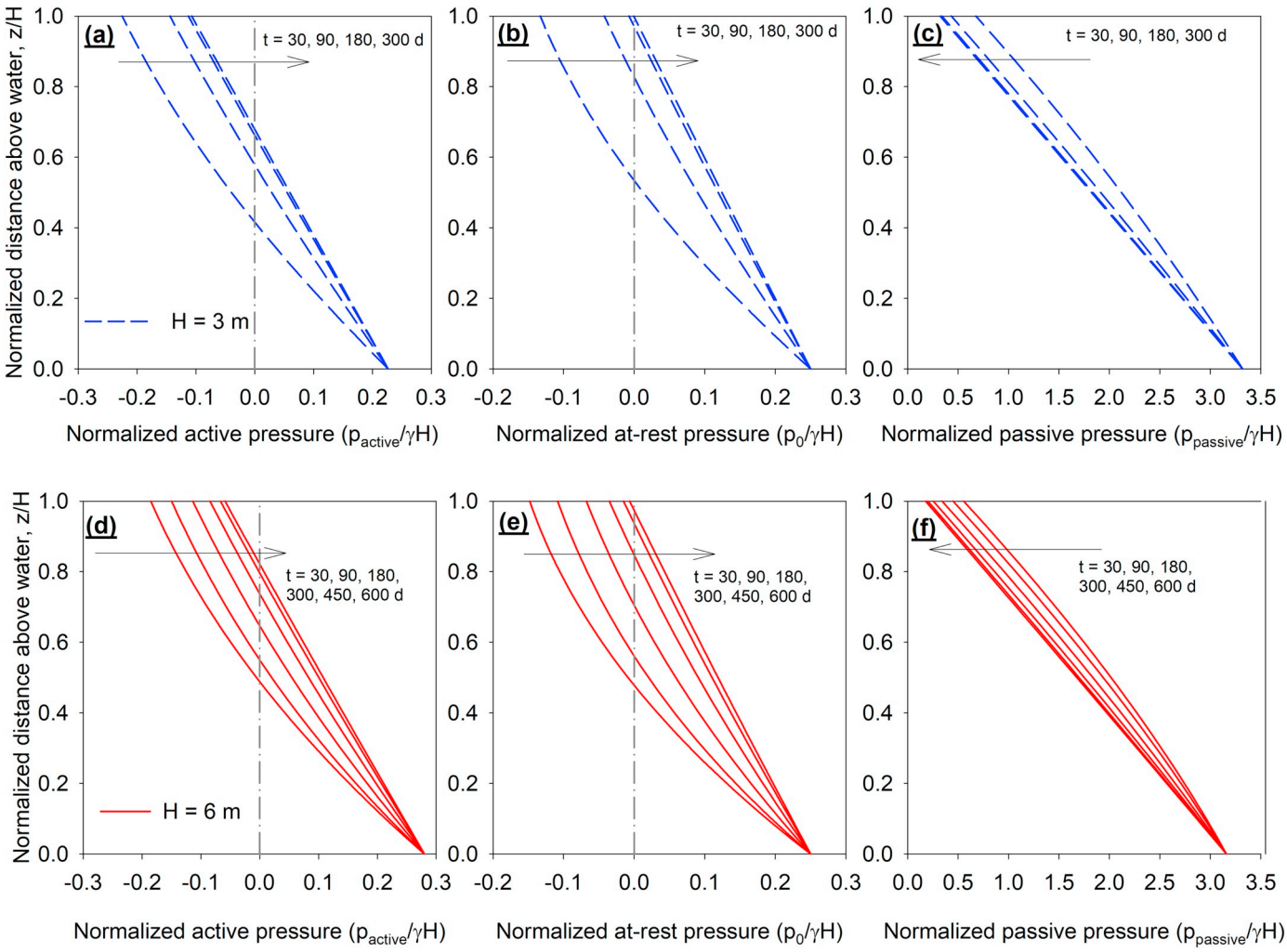

Fig. 6. Normalized profiles of active, at-rest, and passive earth pressures at different times for the clay layer with H = 3 m (top row) and H = 6 m (bottom row).

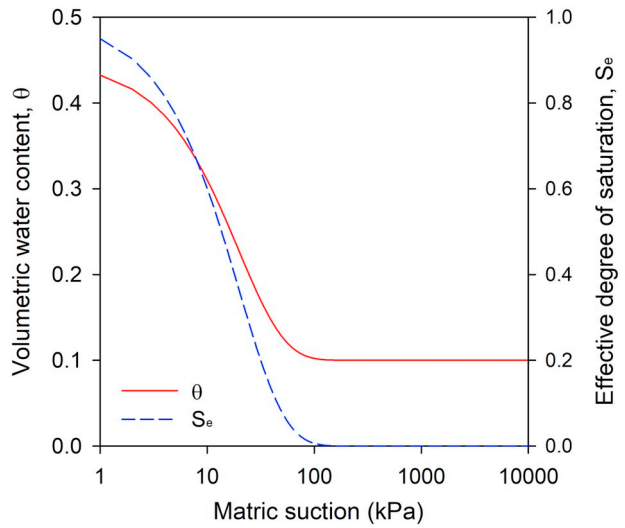

Fig. 7. The SWRC and HCF of silt used in the parametric study.

t = 1 day in the middle of the sand layer as $u_w \approx -10$ and -18 kPa for H = 3 and 6 m, respectively. Further, the pore-water pressure and suction stress trends demonstrate a fast saturation process in comparison with the clay and silt soils, where it takes only 6 and 8 days (not shown) to reach the state of saturation for H = 3 and 6 m, respectively.

The suction stress analysis in the middle of the sand layer for H = 3 m reveals that the normalized σ^s changes from -3.24 to zero in a time span of 5 days, while it changes from -5.5 kPa to zero in 7 days for H = 6 m.

The lateral earth pressure profiles for fine sand is obtained by implementing the acquired suction stress from the previous step in the extended active, at-rest, and passive lateral earth pressure equations. Fig. 12 represents the lateral earth pressure analysis for H = 3 and 6 m. Fig. 12a and d show the time evolution of lateral earth pressure profiles for the active mode for H = 3 and 6 m, respectively. The trends show the nonlinearity in active earth pressure at t = 1 day, but gradually changes to a linear distribution as the pore-water pressure approaches to zero (i.e., saturated condition). The tension zone covers approximately 10% of the sand layer at t = 1 day, but progressively reduces to zero as the sand layer approaches saturated conditions.

Similar trends are also observed for the at-rest earth pressure profiles (Fig. 12b and e), although the level of nonlinearity in the at-rest earth pressure profiles is less than that observed in the active mode. In addition, the difference between lateral earth pressure distribution at t = 1 day and steady-state conditions (saturated condition) for the at-rest mode is less than that in the active mode. Fig. 12c and f show the passive earth pressure profiles for H = 3 and 6 m, respectively. The trends show a narrow range in lateral earth pressure evolution in the passive mode. Although the magnitudes are close in transient (t = 1 day) and steady-state conditions (saturated condition), the earth pressure profile proves to be nonlinear in transient conditions and linear in saturated conditions.

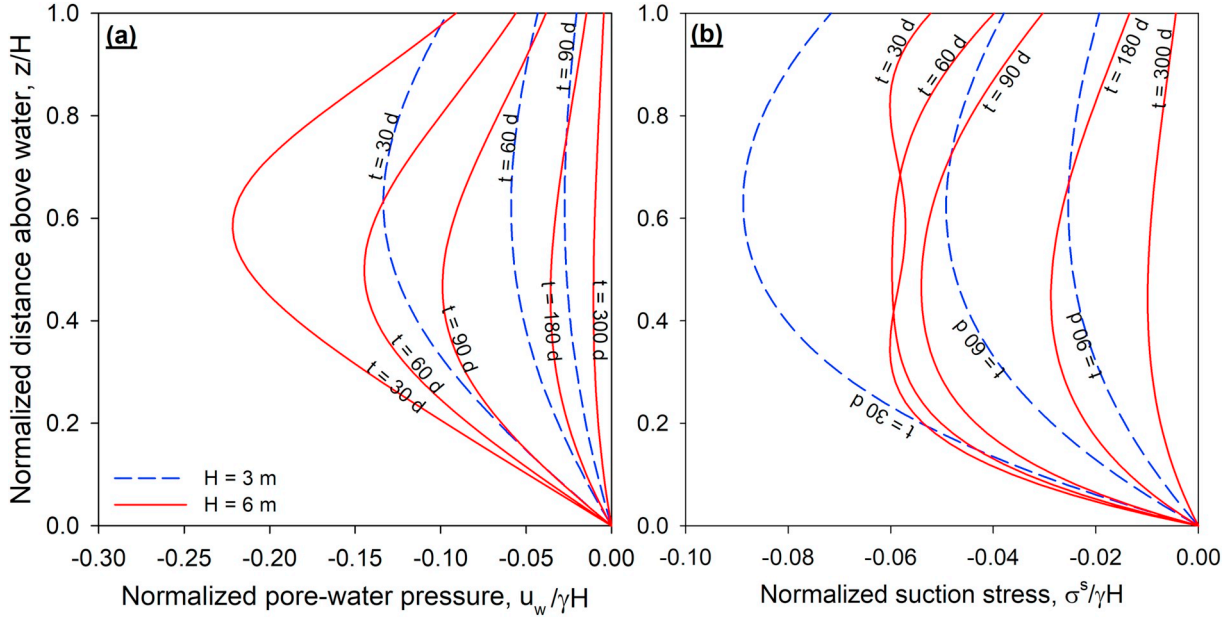

Fig. 8. Transient profiles of normalized distance above the water table in silt versus: (a) normalized pore-water pressure and, (b) normalized suction stress.

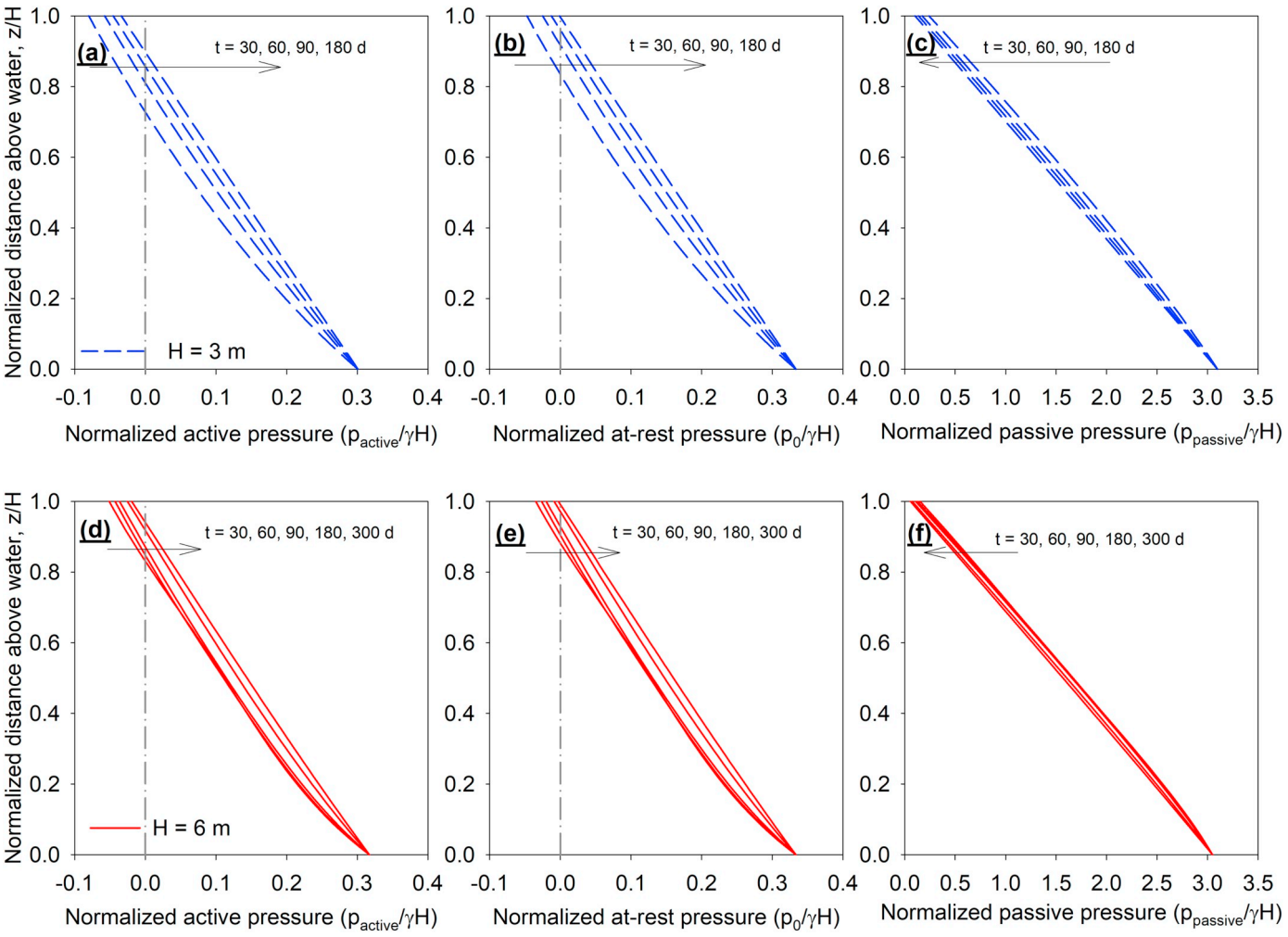

Fig. 9. Normalized profiles of active, at-rest, and passive earth pressures at different times for the silt layer with H = 3 m (top row) and H = 6 m (bottom row).

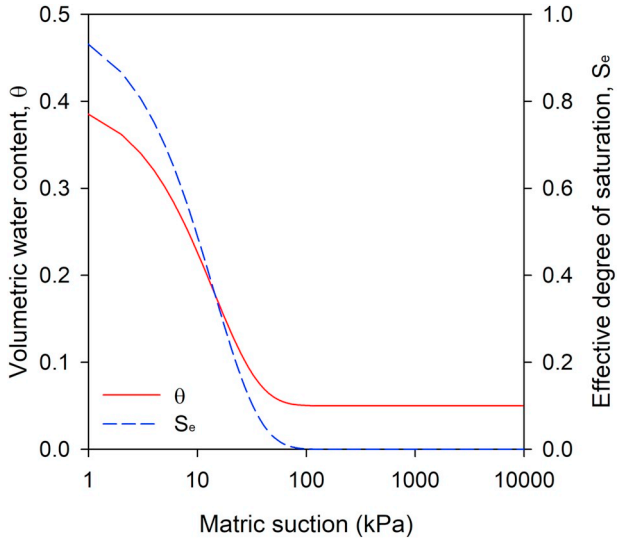

Fig. 10. The SWRC and HCF of fine sand used in the parametric study.

In general, Richards' equation is a nonlinear equation. When used along with Gardner's model, the air entry value (α) is a key parameter that controls the level of nonlinearity. The air entry value (α) strongly depends on the pore size of porous media. Subsequently, α parameter increases transitioning from clay to silt, and to fine sand. Studying the SWRCs of clay, silt, and fine sand shows that the clay transition from a saturated condition to dry condition occurs in a relatively wide range of suction (5 to 500 kPa), while this range is noticeably narrower for silt and fine sand (1 to 90 kPa). The layer thickness is another parameter that contributes to the complexity of the problem. The combination of high values of α and H leads to the trends observed in the suction stress profiles (Fig. 8b and Fig. 11b), where H = 8 m and α = 0.5 and 0.7 1/m for silt and fine sand, respectively.

6. Discussion

Several factors such as soil volumetric dilation, underestimation of soil shear strength, and the effect of suction stress contribute to the performance of slopes and earthen structures but are not considered in the design. While these factors may exist and contribute, they are commonly treated as implicit margin of safety and are not accounted for in design. This is a safe practice primarily since the corresponding values of these factors, in general, cannot be accurately determined for the life span of the structure and they may decrease or diminish in an uncontrolled and random manner. However, quantifying their role can provide invaluable insight into the response of unsaturated earthen structures under normal and extreme loading conditions.

It is well known that suction can have a very important effect on the behavior of unsaturated slopes and earthen structures through its contribution to the soil's shear strength and compressibility. For example, the existence of suction can significantly reduce the lateral thrust in earth retaining systems (Vahedifard et al., 2015) and decrease the mobilized reinforcement force in reinforced walls and slopes (Vahedifard et al., 2016). In design, the contribution of suction is usually ignored, primarily due to uncertainties associated with and huge variation of suction during the life span of structure. The suction contribution can quickly degrade and eventually vanish upon infiltration. An improved understating about the variation of suction becomes even more important for unsaturated earthen structures subjected to extreme precipitations, which cause transient infiltration.

This study presented an analytical solution for modeling earth pressure profiles in unsaturated soils under transient infiltration. The approach provides a rational tool for futures studies to better explain the service state behavior of earthen structures subjected to transient infiltration as well as to evaluate forensics of failed earthen structures. By quantifying the variation of suction and suction stress during transient infiltration, the proposed method and presented results can be employed in future studies for more accurately interpreting field-measured data for back analysis purposes. In reinforced walls and slopes, for example, the presented methodology can help analyze the mobilized force in the reinforcement layers more accurately. Back analysis of field-measured data can be misleading and even unsafe if one attributes the impact of the other factors to the reinforcement contribution.

To the best of the authors' knowledge, the framework presented in this study is the first attempt to develop an analytical solution for the earth pressure profiles of unsaturated soils subjected to transient flow

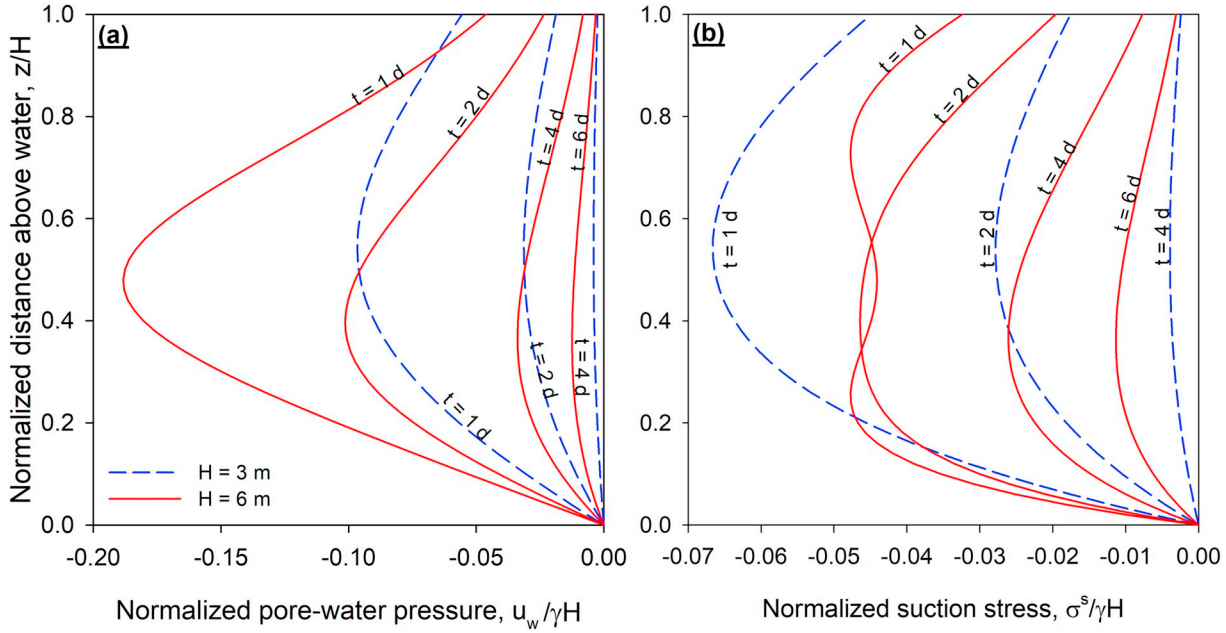

Fig. 11. Transient profiles of normalized distance above the water table in fine sand versus: (a) normalized pore-water pressure and, (b) normalized suction stress distribution.

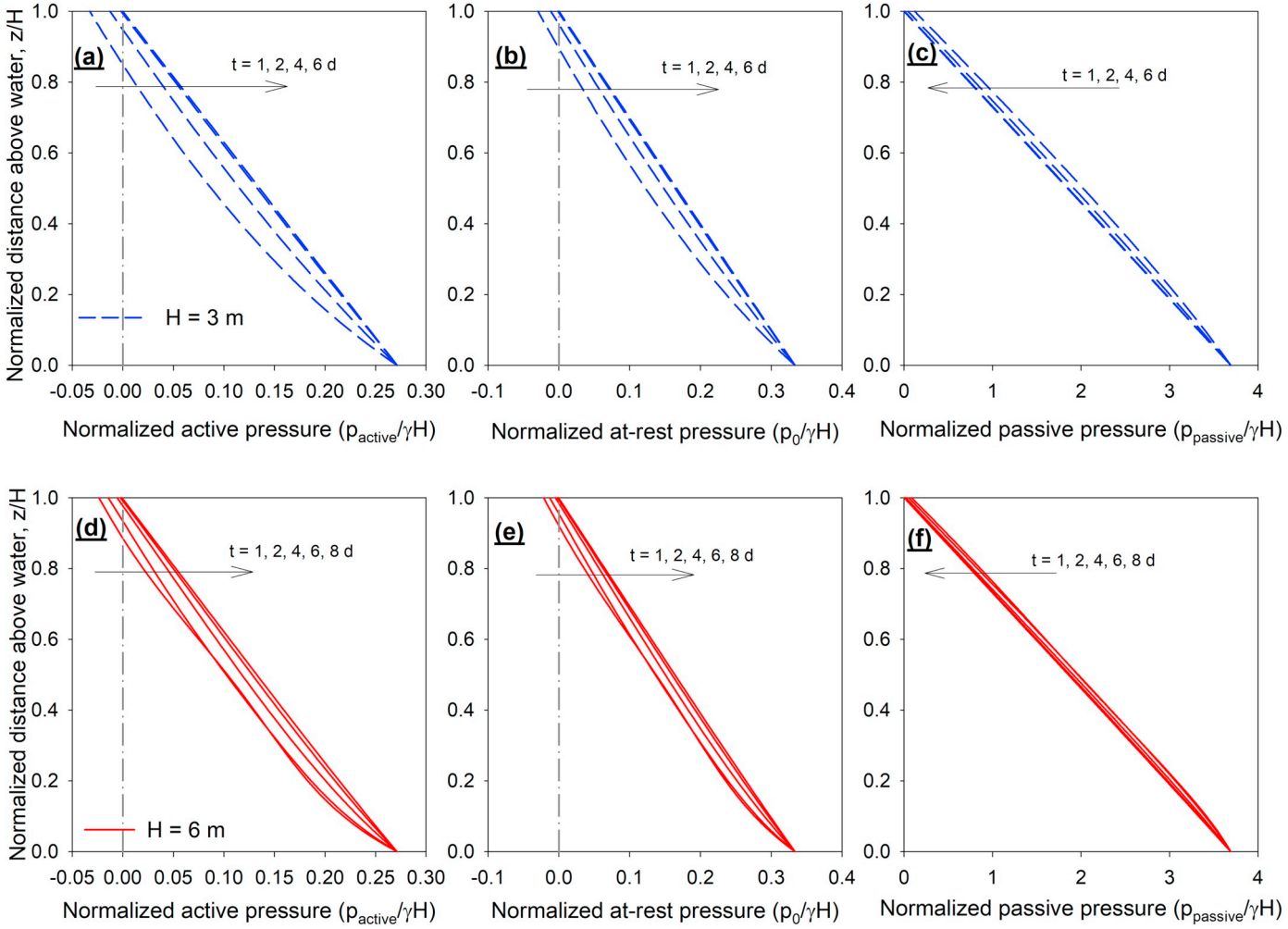

Fig. 12. Normalized profiles of active, at-rest, and passive earth pressures at different times for the fine sand layer with H = 3 m (top row) and H = 6 m (bottom row).

conditions. As almost inherent to any analytical solution, a number of simplifying, yet reasonable, assumptions were employed to derive the analytical solution. The assumptions, while do not invalidate the presented methodology, should be taken into consideration when using and interpreting the results. The assumptions include those used in the classic earth pressure derivations based on Rankine' theory and Hooke's law. Further, a closed-from solution for one-dimensional transient unsaturated flow was used to develop a relatively simple closed-form solution of the suction stress and integrate it into the earth pressure formulation. Such assumption is commonly used in conventional stability and earth pressure methods as well. However, using one-dimensional flow may pose some limitations to accurately capture the variation of suction and suction stress near the face and sharp boundaries of the earth structure. Considering two- or three-dimensional flow requires using more rigorous analytical solutions or using numerical techniques. Another assumption of the proposed formulation lies within one-way coupling of solid-fluid interactions. Accounting for two-way interaction between solids and fluid becomes particularly important for situations where the soil compressibility is considerable and/or the change in total stress is significant. The effect of hydraulic hysteresis is not considered in this study but can be included by adjusting the SWRC fitting parameter for drying and wetting paths (Lu et al., 2013; Likos et al., 2014; Vahedifard et al., 2015).

The study focused on determination of the lateral earth pressure primarily induced by the soil weight under transient flow conditions. In expansive soils, however, there is another stress component imposed by the lateral swelling pressure (e.g., Nelson and Miller, 1992; Liu and Vanapalli, 2017). Expansive soils can swell significantly when subjected to infiltration. The increased lateral swelling pressure can threaten the integrity of earth retaining structures by increasing the driving pressure behind the structure and/or formation of cracks (Nelson and Miller, 1992; Liu and Vanapalli, 2017, 2018). The lateral swelling pressure arises where the volume expansion is horizontally restricted. Determination of the lateral swelling pressure falls beyond the scope of the current study but can be performed using the methods proposed in the literature (e.g., Liu and Vanapalli, 2017, 2018).

Appropriate description of the earth pressure is important not only for soil at or about rest but also for soil and debris in motion. So, the model presented here can be utilized in advanced and sophisticated multi-phase simulations of landslide and debris motion, runout and deposition (e.g., Pudasaini, 2012; Mergili et al., 2017, 2018).

7. Conclusions

Under heavy rainfalls, changes in matric suction and degree of saturation over time and depth can significantly affect earth pressure profiles in unsaturated earthen structures. In this study, an analytical framework was developed to determine the tempo-spatial variation of active, at-rest, and passive earth pressures under transient unsaturated flow. An analytical solution for one-dimensional transient unsaturated flow was integrated into the suction stress-based representation of the effective stress. The formulations were then used to extend Hooke-'s law

to determine at-rest earth pressure and Rankine's theory to obtain active and passive earth pressures of unsaturated soils subjected to transient infiltration.

A parametric study using the proposed formulation showed that in the active mode of earth pressure, the effect of unsteady-unsaturated conditions on clay is considerable. Suction stress is high in the early stages of infiltration and contributes to tension stress. At this condition, the formation of tension cracks in upper layers of the soil near the surface is probable. In early stages of infiltration, the variation of lateral earth pressure is nonlinear in depth and gradually tends to become linear at stages close to steady-state conditions. In the active and at-rest modes, the earth pressure increases with time, but the trend is opposite in the passive mode. The results suggest considering the effect of transient flow on the lateral earth pressure analysis of unsaturated soils, especially for clay in the active and at-rest modes, in which the tension zone has the largest portion of stress distribution in the early stages of infiltration.

Acknowledgments

This material is based upon work supported in part by the National Science Foundation under Grant No. CMMI-1634748. Any opinions, findings, and conclusions or recommendations expressed in this material are those of the author(s) and do not necessarily reflect the views of the National Science Foundation.

References

AASHTO, 2014. AASHTO LRFD Bridge Design Specifications, 7th ed. American Association of State Highway and Transportation Officials, Washington, DC, pp. 2014.
Baum, R.L., Savage, W.Z., Godt, J.W., 2008. TRIGRS—A FORTRAN program for transient rainfall infiltration and grid-based regional slope stability analysis, version 2.0. vol. 2008–1159. U.S. Geol. Surv. Open File Rep, Reston, VA, pp. 74 U.S. Geological Survey.
Bishop, A.W., 1959. The principle of effective stress. Tek Ukeblad 106 (39), 859–863.
Blake, J.R., Renaud, J.P., Anderson, M.G., Hencher, S.R., 2003. Prediction of rainfall-induced transient water pressure head behind a retaining wall using a high-resolution finite element model. Comput. Geotech. 30 (6), 431–442.
Bordoni, M., Meisina, C., Valentino, R., Lu, N., Bittelli, M., Chersich, S., 2015. Hydrological factors affecting rainfall-induced shallow landslides: from the field monitoring to a simplified slope stability analysis. Eng. Geol. 193, 19–37.
CACC (Committee on Adaptation to a Changing Climate), 2015. In: Olsen, J.R. (Ed.), Adapting Infrastructure and Civil Engineering Practice to a Changing Climate. ASCE, Reston, VA.
CACC (Committee on Adaptation to a Changing Climate), 2018. In: Ayyub, B.M. (Ed.), Climate-Resilient Infrastructure: Adaptive Design and Risk Management. ASCE, Reston, VA.
Chen, F.H., 1988. Foundations on Expansive Soils. Elsevier, New York.
Dupuit, J., 1863. Estudes Theoriques et Pratiques sur le Mouvement des Eaux Dans les Canaux Decouverts et a Travers les Terrains Permeables, 2nd ed. Dunod, Paris.
Ering, P., Babu, G.S., 2016. Probabilistic back analysis of rainfall induced landslide-a case study of Malin landslide, India. Eng. Geol. 208, 154–164.
Federal Highway Administration (FHWA), 2009. Mechanically stabilized earth walls and reinforced soil slopes design and construction guidelines. vol. II Technical Rep, Washington, DC FHWA-NHI-10-025.
Fredlund, D.G., Morgenstern, N.R., 1977. Stress state variables for unsaturated soils. J. Geotech. Eng. Div. 103 (5), 447–466 Am. Soc. Civ. Eng.
Fredlund, D.G., Rahardjo, H., 1993. Soil Mechanics for Unsaturated Soils. Wiley, New York.
Gardner, W.R., 1958. Some steady state solutions of the unsaturated moisture flow equation with application to evaporation from a water table. Soil Sci. 85 (4), 228–232.
Gariano, S.L., Guzzetti, F., 2016. Landslides in a changing climate. Earth Sci. Rev. 162, 227–252.
Godt, J.W., Baum, R., Lu, N., 2009. Landsliding in partially saturated materials. Geophys. Res. Lett. 36 (2), L02403.
Godt, J.W., Şener Kaya, B., Lu, N., Baum, R.L., 2012. Stability of infinite slopes under transient partially saturated seepage conditions. Water Resour. Res. 48 (5), W05505.
IPCC, 2013. Climate Change 2013: the physical science basis. In: Contribution of Working Group I to the Fifth Assessment Report of the Intergovernmental Panel on Climate Change. Cambridge University Press, Cambridge, United Kingdom and New York, NY, USA, pp. 1535.
Jasim, F.H., Vahedifard, F., Ragno, E., AghaKouchak, A., Ellithy, G., 2017. Effects of climate change on fragility curves of earthen levees subjected to extreme precipitations. In: *Geo*-Risk 2017: Geotechnical Risk from Theory to Practice, GSP No. 285, June 4–6. vol. 2017. pp. 498–507 Denver, CO.
Kim, S.K., Borden, R.H., 2013. Numerical simulation of MSE wall behavior induced by surface-water infiltration. J. Geotech. Geoenviron. Eng. 139 (12), 2110–2124.
Larsen, M.C., 2008. Rainfall-triggered landslides, anthropogenic hazards, and mitigation strategies. Adv. Geosci. 14, 147–153.
Leshchinsky, D., Tatsuoka, F., 2013. Performance, design, and redundancy, Geosynthetic reinforced walls in the public sector. Geosynthetics 31 (3), 12–21.
Leshchinsky, B., Vahedifard, F., Koo, H.-B., Kim, S.-H., 2015. Yumokjeong Landslide: an Investigation of progressive failure of a Hillslope using the Finite Element Method. Landslides 12 (5), 997–1005.
Li, Z., Yang, X.L., 2018. Active earth pressure for soils with tension cracks under steady unsaturated flow conditions. Can. Geotech. J. https://doi.org/10.1139/cgj-2017-0713.
Li, J., Xingand, T., Hou, Y., 2014. Centrifugal model test on the at-rest coefficient of lateral earth pressure in unsaturated soils. In: Proceedings of the 8th International Conference on Physical Modelling in Geotechnics, pp. 931–936 Perth.
Liang, W., Zhao, J., Li, Y., Zhang, C., Wang, S., 2012. Unified solution of Coulomb's active earth pressure for unsaturated soils without crack. Appl. Mech. Mater. 170–173, 755–761.
Likos, W., Lu, N., Godt, J., 2014. Hysteresis and uncertainty in soil water-retention curve parameters. J. Geotech. Geoenviron. Eng. 140 (4), 04013050.
Liu, Y., Vanapalli, S.K., 2017. Influence of lateral swelling pressure on the geotechnical infrastructure in expansive soils. J. Geotech. Geoenviron. Eng. 143 (6), 04017006.
Liu, Y., Vanapalli, S.K., 2018. Prediction of lateral swelling pressure behind retaining structure with expansive soil as backfill. Soils Found. https://doi.org/10.1016/j.sandf.2018.10.003.
Lu, N., Godt, J.W., 2013. Hillslope Hydrology and Stability. Cambridge University Press.
Lu, N., Likos, W., 2004. Unsaturated Soil Mechanics. John Wiley and Sons, Inc, Hoboken, New Jersey.
Lu, N., Likos, W.J., 2006. Suction stress characteristic curve for unsaturated soil. J. Geotech. Geoenviron. Eng. 132 (2), 131–142.
Lu, N., Godt, J.W., Wu, D.T., 2010. A closed-form equation for effective stress in unsaturated soil. Water Resour. Res. 46 (5), W05515.
Lu, N., Kaya, M., Collins, B.D., Godt, J.W., 2013. Hysteresis of unsaturated hydromechanical properties of a silty soil. J. Geotech. Geoenviron. Eng. 139 (3), 507–510.
Mergili, M., Jan-Thomas, F., Krenn, J., Pudasaini, S.P., 2017. r. Avaflow v1, an advanced open-source computational framework for the propagation and interaction of two-phase mass flows. Geosci. Model Dev. 10 (2), 553.
Mergili, M., Emmer, A., Juřicová, A., Cochachin, A., Fischer, J.T., Huggel, C., Pudasaini, S.P., 2018. How well can we simulate complex hydro-geomorphic process chains? the 2012 multi-lake outburst flood in the Santa Cruz Valley (Cordillera Blanca, Perú). Earth Surf. Process. Landf. 43 (7), 1373–1389.
Monoroy, R., Zdravkovic, L., Ridley, A., 2015. Mechanical behaviour of unsaturated expansive clay under K0 conditions. Eng. Geol. 197, 112–131.
Nelson, J.D., Miller, J.D., 1992. Expansive Soils, Problems and Practice in Foundation and Pavement Engineering. Wiley Press, New York.
NRC, 2013. Abrupt impacts of climate change: anticipating surprises, committee on understanding and monitoring abrupt climate change and its impacts. In: Board on Atmospheric Sciences and Climate, Division on Earth and Life Studies, pp. 250 Washington, DC.
Oh, S., Lu, N., 2015. Slope stability analysis under unsaturated conditions: case studies of rainfall-induced failure of cut slopes. Eng. Geol. 184, 96–103.
Oh, S., Lu, N., Kim, T., Lee, Y., 2013. Experimental validation of suction stress characteristic curve from nonfailure triaxial k_0 consolidation tests. J. Geotech. Geoenviron. Eng. 139 (9), 1490–1503.
Özışık, M.N., 1980. Heat Conduction. John Wiley & Sons.
Petley, D., 2012. Global patterns of loss of life from landslides. Geology 40 (10), 927–930.
Pham, K., Kim, D., Choi, H.J., Lee, I.M., Choi, H., 2018. A numerical framework for infinite slope stability analysis under transient unsaturated seepage conditions. Eng. Geol. 243, 36–49.
Pudasaini, S.P., 2012. A general two-phase debris flow model. J. Geophys. Res. 117, F03010. https://doi.org/10.1029/2011JF002186.
Pudasaini, S.P., 2016. A novel description of fluid flow in porous and debris materials. Eng. Geol. 202, 62–73.
Ragno, E., AghaKouchak, A., Love, C.A., Cheng, L., Vahedifard, F., Lima, C.H.R., 2018. Quantifying changes in future intensity-duration-frequency curves using multi-model ensemble simulations. Water Resour. Res. 54 (3), 1751–1764.
Rahardjo, H., Satyanaga, A., Leong, E.C., Ng, Y.S., Pang, H.T.C., 2012. Variability of residual soil properties. Eng. Geol. 141–142, 124–140.
Rahimi, A., Rahardjo, H., Leong, E.-C., 2010. Effect of hydraulic properties of soil on rainfall-induced slope failure. Eng. Geol. 114, 135–143.
Richards, L.A., 1931. Capillary conduction of liquids through porous mediums. J. Appl. Phys. 1, 318–333.
Robinson, J.D., Vahedifard, F., AghaKouchak, A., 2017. Rainfall-triggered Slope Instabilities under a changing climate: comparative Study using Historical and projected Precipitation Extremes. Can. Geotech. J. 54 (1), 117–127.
Sahoo, J.P., Ganesh, R., 2017. Active earth pressure on retaining walls with unsaturated soil Backfill. In: International Congress and Exhibition Sustainable Civil Infrastructures: Innovative Infrastructure Geotechnology. Springer, Cham, pp. 1–19.
Sorbino, G., Nicotera, M.V., 2013. Unsaturated soil mechanics in rainfall-induced flow landslides. Eng. Geol. 165, 105–132.
Srivastava, R., Yeh, T.C.J., 1991. Analytical solutions for one-dimensional, transient infiltration toward the water table in homogeneous and layered soils. Water Resour. Res. 27 (5), 753–762.
Tang, G., Huang, J., Sheng, D., Sloan, S.W., 2018. Stability analysis of unsaturated soil slopes under random rainfall patterns. Eng. Geol. 245, 322–332.
USGCRP (U.S. Global Change Research Program), 2009. Global Climate Change Impacts

in the United States. Cambridge University Press, Washington, DC.
Vahedifard, F., Leshchinsky, B.A., Sehat, S., Leshchinsky, D., 2014. Impact of cohesion on seismic design of geosynthetic-reinforced earth structures. J. Geotech. Geoenviron. 140 (6), 04014016.
Vahedifard, F., Leshchinsky, B.A., Mortezaei, K., Lu, N., 2015. Active earth pressures for unsaturated retaining structures. J. Geotech. Geoenviron. Eng. 141 (11), 04015048.
Vahedifard, F., Mortezaei, K., Leshchinsky, B.A., Leshchinsky, D., Lu, N., 2016. Role of suction stress on service state behavior of geosynthetic-reinforced soil structures. Transport. Geotech. 8, 45–56.
Vahedifard, F., AghaKouchak, A., Ragno, E., Shahrokhabadi, S., Mallakpour, I., 2017a. Lessons from the Oroville Dam. Science 355 (6330), 1139–1140.
Vahedifard, F., Tehrani, F.S., Galavi, V., Ragno, E., AghaKouchak, A., 2017b. Resilience of MSE Walls with marginal Backfill under a changing climate: Quantitative Assessment for Extreme Precipitation events. J. Geotech. Geoenviron. Eng. 143 (9), 04017056.
Vahedifard, F., Williams, J.M., AghaKouchak, A., 2018. Geotechnical Engineering in the Face of Climate Change: Role of Multi-Physics Processes in Partially Saturated Soils. *Proc. IFCEE 2018*, GSP No. 295. pp. 353–364.
Vardon, P.J., 2015. Climatic influence on geotechnical infrastructure: a review. Environ. Geotech. 2 (3), 166–174.
Vo, T., Russell, A.R., 2014. Slip line theory applied to a retaining wall–unsaturated soil interaction problem. Comput. Geotech. 55, 416–428.
Vo, T., Taiebat, H., Russell, A.R., 2016. Interaction of a rotating rigid retaining wall with an unsaturated soil in experiments. Géotechnique 66 (5), 366–377.
Yang, K., Thuo, J., Chen, J., Liu, C., 2018. Failure investigation of a geosynthetic-reinforced soil slope subjected to rainfall. Geosynth. Int. https://doi.org/10.1680/jgein.18.00035.
Yeh, T.C.J., 1989. One-dimensional steady state infiltration in heterogeneous soils. Water Resour. Res. 25 (10), 2149–2158.
Yelti, N., 2011. Analysis and Design of Soil Nail Walls in High Plasicity Clays. M.S. thesis. The University of Texas at San Antonio, TX.
Yoo, C., Jung, H., 2006. Case history of geosynthetic reinforced segmental retaining wall failure. J. Geotech. Geoenviron. Eng. 132 (12), 1538–1548.
Zhang, R., Zheng, J., Yang, H., 2009. Experimental study on k_0 consolidation behavior of recompacted unsaturated expansive soil. In: Proceedings of GeoHunan International Conference, pp. 27–32 Changsha, Hunan.
Zhang, C., Zhao, J., Zhang, Q., Xu, F., 2010. Unified solutions for unsaturated soil shear strength and active earth pressure. In: Hoyos, L.R., Zhang, X., Puppala, A.J. (Eds.), Experimental and applied modeling of unsaturated soils, Geotechnical Special Publication No. 202. ASCE, Reston, VA, pp. 218–224.
Zhang, X., Alonso, E.E., Casini, F., 2016. Explicit formulation of at-rest coefficient and its role in calibrating elasto-plastic models for unsaturated soils. Comput. Geotech. 71, 56–68.